Title: DNA impedance biosensor for detection of cancer, *TP53* gene mutation, based on gold nanoparticles/aligned carbon nanotubes modified electrode

Author: H. Fayazfar A. Afshar M. Dolati A. Dolati

PII: S0003-2670(14)00637-0
DOI: http://dx.doi.org/doi:10.1016/j.aca.2014.05.029
Reference: ACA 233273

To appear in: *Analytica Chimica Acta*

Received date: 22-3-2014
Revised date: 6-5-2014
Accepted date: 16-5-2014

Please cite this article as: H.Fayazfar, A.Afshar, M.Dolati, A.Dolati, DNA impedance biosensor for detection of cancer, TP53 gene mutation, based on gold nanoparticles/aligned carbon nanotubes modified electrode, Analytica Chimica Acta http://dx.doi.org/10.1016/j.aca.2014.05.029

DNA impedance biosensor for detection of cancer, *TP53* gene mutation, based on gold nanoparticles/ aligned carbon nanotubes modified electrode

H. Fayazfar [b], A. Afshar[b], M. Dolati[a, *], A. Dolati[b]

[a] bioscience and biotechnology Research Center, Qom University of Medical Sciences, Qom, Iran

[b]Materials Science and Engineering Department, Sharif University of Technology, Tehran, P.O.BOX 11155-9466, I.R.Iran

[*] Corresponding author. Tel:+989126529172 . E-mail address: k_dolati_m@yahoo.com (M. Dolati)

For the first time, a new platform based on electrochemical growth of Au nanoparticles on aligned multi-walled carbon nanotubes (A-MWCNT) was developed for sensitive lable-free DNA detection of the *TP53* gene mutation, one of the most popular genes in cancer research. Electrochemical impedance spectroscopy (EIS) was used to monitor the sequence-specific DNA hybridization events related to *TP53* gene. Compared to the bare Ta or MWCNT/Ta electrodes, the synergistic interactions of vertically aligned MWCNT array and gold nanoparticles at modified electrode could improve the density of the probe DNA attachment and resulting the sensitivity of the DNA sensor greatly. Using EIS, over the extended DNA concentration range, the change of charge transfer resistance was found to have a linear relationship in respect to the logarithm of the complementary oligonucleotides sequence concentrations in the wide range of 1.0×10^{-15}–1.0×10^{-7} M, with a detection limit of 1.0×10^{-17} M (S/N=3). The prepared sensor also showed good stability (14 days), reproducibility (RSD=2.1%) and could be conveniently regenerated via dehybridization in hot water. The significant improvement in sensitivity illustrates that combining gold nanoparticles with the on-site fabricated aligned MWCNT array represents a promising platform for achieving sensitive biosensor for fast mutation screening related to most human cancer types.

Keywords: Gold nanoparticle, Hybridization, Electrochemical impedance sensor, Multi-walled carbon nanotube, gene mutation

1. Introduction

The tumour suppressor gene *TP53* is mutated in most type of human cancers and is one of the most popular genes in cancer research. Moreover, many studies have suggested that *TP53* mutations have prognostic importance and sometimes are a significant factor in determining the response of tumours to therapy [1]. For these reasons, *TP53* is an important early diagnostic cancer marker. The human *TP53* is located on chromosome 17 (17p13.1) and has a wide spectrum of mutations in human tumours [2]. Aggressive growth of several types of cancer has been attributed to mutations in this gene. Sequence-specific analysis of the *TP53* gene can thus become extremely useful to assist monitoring of cancer progress and patient therapy. According to the above items, it is of considerable interest to search a highly sensitive and selective biosensor for early stage cancer diagnosis. In addition, human gene research shows that gene mutations often cause genetic disease to happen. Therefore, it is important to develop rapid DNA-detection methods for life science research and clinical diagnosis of pathogenic and genetic diseases [3].

A variety of methods are currently used to assess the *TP53* status of individual tumours, recently reviewed by Jiang et al [4]. Many efforts have been made to develop fast and inexpensive methods for *TP53* mutations detection based on biosensors and gene chips. In particular, different transduction principles, optical (surface plasmon resonance-SPR) and piezoelectric, have been already applied to *TP53* mutation detection [5-9]. All the systems are based on the hybridization reaction between a probe immobilized on the sensing surface and the complementary sequence or the mismatch one in solution. Among the existing approaches, electrochemical DNA biosensors have displayed an exceptional development in recent years. Today these devices allow a simple, fast, and sensitive detection of hybridization events without using any expensive and time-consuming readout techniques. In the reported sensors for *TP53* in electrochemical sensing, the probe was immobilized on a carbon paste electrode [8,9] or a gold electrode [10]. However, for the application of earlier diagnosis, where the analyte concentration is very low, developing a simple, rapid, low-cost and highly sensitive and selective assay platform remains a challenging and critical subject for TP53 mutation detection [11-14].

In addition, a key issue with any DNA hybridization biosensor is how to enhance the probe DNA immobilization amount, and maintain the accessibility of probe DNA for hybridization detection. Recent advances in nano materials science offered unforeseeable opportunity of making new sensitive biosensors [15]. Earlier studies have explored using carbon nanotubes [16,17] and/or gold nanoparticles (AuNPs) [18,19] to detect DNA and achieved favorable results. The Xu and Fang group showed, for example, that CdS nanoparticles could be utilized for signal amplification, which lowered the detection limit down to 1.43×10^{-10} M [20]. The Li and Zhang group utilized gold nanoparticles electrodeposited on the glassy carbon electrode for the immobilization of the thiolated aptamer, and achieved the lowest detection limit of 0.03 nM [21]. Carbon nanotubes are ideal electrodes for constructing advanced biosensors. In this regard, both protein and DNA chains have been chemically attached onto either nonaligned or aligned carbon nanotubes [22-24]. The use of aligned carbon nanotubes provides additional advantages for a maximized access of the nanotube electrode surface and an efficient device construction. On the other hand, the fact that gold nanoparticles are able to provide a stable immobilization of

biomolecules that retain their bioactivity is a major advantage for the preparation of biosensors [25]. Also AuNPs are physically flexible and suitable for immobilization of DNA without losing its conformation or biological activity. So nanocomposite electrochemical sensors with nanostructured surfaces do not only offer significantly increased surface area for attaching probe molecules, but also exhibit improved electrochemical properties and beneficial orientation effects in probe immobilization so that they encouraged us to develop a highly sensitive *TP53* sensor based on the synergistic effect of Au nanoparticles and aligned multi-walled carbon nanotubes (A-MWCNTs) for the first time in this work.

A convenient electrochemical technique is electrochemical impedance spectroscopy (EIS), widely applied in DNA detection. EIS [26–28] is known as a label-free and non-destructive technique because of the characterization of the electrochemical properties of biological interfaces and their ability to determine low levels of the analyte bound to the sensor surface. Park and co-worker have recently reviewed progresses on EIS based DNA hybridization sensors [29].

This research was attempted to construct a new highly sensitive label-free platform to detect specific sequence of *TP53* gene through electrochemically growing Au NPs on the vertically aligned MWCNT array which, to best of our knowledge, have not been reported before. A probe DNA (26-mer) modified with –SH was first adsorbed chemically on the aligned MWCNTs and gold nanoparticles through self-assembly. The target DNA, which contains complementary sequence to the probe DNA, would be captured by the probe DNA through hybridization. In order to evaluate the electrochemical characteristics of the modified electrode, $[Fe(CN)_6]^{3-/4-}$ was used as a probe in cyclic voltammetry (CV) and electrochemical impedance spectroscopic measurements. Remarkably, the obtained DNA biosensor exhibited excellent response to target DNA related to *TP53* mutation detection.

2.Experimental:

2.1. Electrochemical measurements

The electrochemical measurements were performed with a potentiostat–galvanostat AutoLab electrochemical analysis system supplied with a FRA 2.0 module (Echo Chemie BV Model PGSTAT-302N, Netherlands) with a three-electrode cell containing a saturated calomel electrode (SCE) as a reference electrode and a platinum wire as an auxiliary electrode. Tantalum electrodes (0.75 cm^{-2}), unmodified or modified with aligned MWCNT/AuNPs or DNA modified A-MWCNT/AuNPs were applied as working electrodes. CV and EIS were performed in a solution containing 5.0 mM $K_3[Fe(CN)_6]/K_4[Fe(CN)_6]$ and 0.10 M KCl . The EIS measurements were recorded within the frequency range of 1 mHz to 10 kHz at a potential of 0.17 V and a voltage amplitude of 5 mV. In the CV studies, the potential was cycled from -0.1 to 0.7 V with a scan rate of 5 mV s^{-1}. Field emission scanning electron microscope (FESEM) (MIRA TESCAN operating at 20 kV) was used to observe the morphology and nanostructures of the prepared A-MWCNTs electrodes (modified and unmodified). Transmission electron microscope (TEM) measurements were performed with a Philips EM 208 FEG instrument operating at 90 kV.

2.2. Reagents

All used chemicals were of analytical grades, and doubly distilled water was used throughout. Analytical grade $HAuCl_4 \cdot 4H_2O$, $K_{3,4}[Fe(CN)_6]$ and trishydroxymethyl aminomethane were purchased from Sigma. All oligonucleotide fragments used in this study were purchased from FAZA Biotech (Iran). Thiolated oligonucleotides with a mercaptohexyl group at each 5´-

phosphate end, abbreviated as HS–$(CH_2)_6$-ssDNA, were used as received. Their sequences are the following (probe DNA):
26-mer 5´-SH-$(CH_2)_6$-TGG GCG GCA TGA ACC GGA GGC CCA TC-3´;
The complementary sequence DNA (target DNA): a 26-base fragment of *TP53* gene sequence of 5´- GAT GGG CCT CCG GTT CAT GCC GCC CA -3´; 1-base mismatched DNA with the sequence of 5´ GAT GGG CCT CTG GTT CAT GCC GCC CA-3´; and 3-base mismatched DNA with the sequence of 5´ GAT CGG CCT CTG GTT CTT GCC GCC CA-3´. 50 mM Tris-HCl buffer solution with different pH levels was prepared by mixing different volumes of 0.1 M trishydroxymethyl-aminomethane and 0.1 M HCl with water.

2.3. Fabrication of A-MWCNT/AuNPs electrode

Well-aligned MWCNTs were synthesized on Ni-deposited Ta plates by chemical vapor deposition (CVD) with ethylenediamine as a precursor. Briefly, the 0.01-1 M ethanol solution of metal salt $NiCl_2.6H_2O$, has been prepared in an argon (Ar)-filled glovebox. After that, Ta substrate was coated (sprayed) with drops of metal chloride solution and was dried by Ar. The Ni coated Ta plates were directly put into the middle of the quartz tube reactor that was preheated to 850 ^oC. The substrates were pretreated by N_2 with a flow rate of 500 sccm for 5 min, forming the nano sized catalytic particles. After purging and preheating with N_2, the ethylenediamine was introduced by bubbling N_2 at a flow rate of 500 sccm through liquid ethylenediamine contained in a glass bottle, thus the formed feeding gas contained approximately 8% ethylenediamine. The reaction times were varied from 5 to 45 min, after which the reactor was cooled down to room temperature in N_2 ambient. By altering the growth time and catalyst thickness, well-aligned MWCNTs with uniform size and good distribution were produced. To electrochemically purify CNTs with keeping their alignment and introducing hydroxyl and carboxyl functional groups to them, the MWCNTs electrode was immersed in 0.2 M HNO_3 solution and the potential was cycled between +1.00 and +2.00 V at a scan rate of 50 mV s^{-1}. An oven drying technique (80-100 ^oC) retained the vertically aligned and laterally spaced geometry of these CNT arrays after being subjected to the electrochemical modification. Then electrodeposition of gold nanoparticles (AuNPs) on CNT arrays was performed by the potential step technique (chronoamperometry) from an acidic solution of 0.5 M H_2SO_4 containing 5 mM $HAuCl_4$. The applied potential was stepped from +0.80 V where no Au is deposited on the electrode surface to +0.20 V during 10 s. The obtained A-MWNTs/Au modified electrodes were washed carefully in deionized water, then were dried at room temperature. The as-fabricated electrodes (A-MWCNTS/Au NPs/TaE) were utilized for electrochemical measurement and further analysis.

2.4. Fabrication of ssDNA electrochemical biosensor and hybridization of ssDNA modified electrode.

The freshly obtained A-MWCNT/AuNPs/Ta electrode was incubated at 4 ^oC in a 50 mM Tris–HCl buffer solution (pH 8.0) containing 1.0 µM probe DNA for 10 h. During this process the single-stranded DNA (ssDNA) self-assembled on the MWCNT-Au electrode. Afterwards, the A-MWCNT/AuNPs/ssDNA/Ta electrode was carefully washed with doubly distilled water to remove any trace of unassembled probe ssDNA. The thus-obtained electrode is denoted as A-MWCNT/AuNPs/ssDNA/TaE in this study. DNA hybridization of the A-MWCNT/ AuNPs/ssDNA/Ta electrode was carried out by immersing it in a target DNA solution of various concentrations at 42 ^oC for 2 h (A-MWCNT/AuNPs/dsDNA/TaE). After that, the hybridized

electrode was thoroughly rinsed with a 0.2% sodium dodecylsulfate phosphate buffer (pH 7.3) to remove nonhybridized target DNA, then washed with doubly distilled water to remove phosphate buffer. Scheme 1 illustrates how the DNA-functionalized A-MWCNT/AuNPs platform was constructed in this research.

Electrodes with DNA self-assembly of different surfaces density were also interrogated in this work. Low-density surfaces (1.2×10^{12} molecule/cm^2) were obtained by incubation of electrodes with 1.0 μM of capture probes in the immobilization buffer for 10 h. Respectively, medium-density (6.0×10^{12} molecule/cm^2) and high-density (1.2×10^{13} molecule/cm^2) surfaces were prepared by incubation of electrodes with 2 and 5 μM of capture probes in the immobilization buffer for 14 h.

Scheme 1.

3. Results and discussion

3.1. Characterization of the well aligned MWCNTs on the Ta substrate

Four different methods including SEM, TEM, CV and EIS were used to investigate the optimization of the nanosensor.

Fig. 1A and B shows SEM images of the grown well aligned CNTs on the polished Ta substrate at 850 ^{o}C after 6 min. Regarding to investigation of different parameters on the CNTs growth and alignment, it was observed that well aligned CNTs with diameter between 20 to 100 nm and length of several micrometers were produced on a conductive Ta substrate. Fig. 1C and D also show TEM images of the vertically aligned CNTs. In the Fig. 1C it can be observed that tips of the CNTs are closed. No catalyst particle can be observed on the tip of the CNTs indicating that root growth was dominant in which catalyst particles are kept stuck on to the substrate surface. Also, in Fig. 1D it can be seen that CNTs have bamboo-like structures and achieved CNTs are multi-layered.

Fig. 1

3.2. Deposition of the gold nanoparticles on well-aligned MWCNTs by using an electrochemical method

After electrochemical modification of the CNTs in HNO_3 (0.2 M), purification and adding up functional groups; gold nanoparticles were deposited on CNTs using chronoamperometry (potential-step method). Fig. 2 (A) shows chronoamperometric curve for electrochemical deposition of AuNPs on the A-CNTs electrode in 0.5 M H_2SO_4 solution containing 5 mM $HAuCl_4$ at a constant potential of +0.2 V and time of 10 s in which the current density increases at initial stages due to the nucleation and growth process and then drops by increasing the concentration gradient of electroactive species on the surface (i.e. growing the diffusion layer into the solution) [30].

The electrode potential was stepped from an initial potential of +0.8 V, where no reaction occurred, to +0.20 V, at which $AuCl_4^-$ was reduced to Au nanocrystals. Presumably, the reduction of $AuCl_4^-$ to Au^0 begins at surface defect sites where oxygen-containing functional groups, such as carboxylate, serve as axial ligands. Fig. 2 (B) shows SEM image of precipitated AuNPs on the vertically aligned CNTs under these experimental conditions. As it can be seen spherical nanoparticles with small diameters and high density (5.12×10^{11} particles/cm^2) were well dispersed on CNTs which is related to the nucleation of Au nanoparticles at the dense edge-plane-like defects of MWCNT and also it displays a three-dimensional growth of these AuNPs and clusters on the active sites. In some cases, AuNPs completely cover the CNTs surfaces and in some other points aggregate of nanoparticles can be observed considering that some particles

grew more rapidly and over lapped with other particles. Also Fig. 2 (C) depicts the SEM images of the deposited AuNPs on the A-CNTs from the side view. As it can be seen nanoparticles with appropriate density are uniformly precipitated on the A-CNTs without violating CNTs alignment. The average diameter of these AuNPs ranged from 20 to 100 nm. The energy dispersive X-ray (EDX) spectrum and x-ray diffraction (XRD) furtherly confirm the successful growth of Au NPs on aligned MWCNTs (data not shown here).

Fig. 2

3.3. Voltammetric investigations at different Modified Electrodes

Cyclic voltammogram of a redox couple ($Fe(CN)_6^{4-/3-}$) was selected as a probe and redox active indicator to investigate the characteristics of the modified electrode in each modification step. Fig. 3 compares the cyclic voltammograms of 5.0 mM $K_4Fe(CN)_6/K_3Fe(CN)_6$ at different modified electrodes at a scan rate of 5 mVs^{-1}. As it can be seen in Fig. 3(i) at bare Ta electrode no redox probe reaction ($Fe^{3+} + e \leftrightarrow Fe^{2+}$) was occurred and the bare Ta electrode gave a very poor current response in the range of μAcm^{-2}. By modification of the bare Ta electrode with vertically aligned MWCNTs (Fig. 3(iii)) a couple of redox peak appears which is attributed to the redox probe reaction at the electrode surface with a peak-to-peak separation of 200 mV. When AuNPs were electrodeposited on the surface of the A-MWCNT/Ta electrode (curve (iv)), the redox probe reaction at the A-MWCNT/AuNPs/TaE is significantly improved, reflected by the enlarged peak current and the decreased peak-to-peak separation of 110 mV in contrast to the A-MWCNT/Ta electrode (curve (iii)). The decrease of peak-to-peak potential separation in addition to enhancement in peak current sharpness and amount at this modified electrode show a strong catalytic function due to the synergistic effect of the A-MWCNTs and AuNPs towards the redox reaction of probe. The A-MWCNTs and AuNPs can improve the electron transfer rate from Fe ions to the electrode surface due to regular porous structure of CNTs, high electroactive surface areas of A-MWCNTs/AuNPs and the enhanced conductive paths. The large active surface area created by the simultaneous presence of A-MWCNTs and AuNPs dispersed on the surface of CNTs enhance the electrochemical reaction and increase the rate of the heterogeneous electron transfer; thus it obviously increased current response towards the redox probe reaction.

Also Fig. 3(ii) shows the cyclic voltammograms of $Fe(CN)_6^{4-/3-}$ at random-distributed MWCNTs powder electrode. It can be seen that a couple of redox peak appears but the peak current of the redox couple surface decreased in comparison to vertically aligned MWCNTs electrode with an increased peak-to-peak separation of 300 mV. So Well-aligned but mutually separated MWCNTs, offer distinct advantages over loose and randomly oriented CNT powders to effectively increase electrocatalytic activity because they have high surface area which can promote electron transfer due to their regular porous structure and conductive paths.

Fig. 3

Cyclic voltammogram of a redox couple ($Fe(CN)_6^{4-/3-}$) was selected as a probe to investigate the characteristics of the modified electrode in each assembly step of DNA on the electrode. The redox couple $[Fe(CN)_6]^{3-}/[Fe(CN)_6]^{4-}$ showed a reversible behavior at A-MWCNT/AuNPs/Ta electrode with a peak-to-peak separation of 110 mV (Fig. 4(i)). The covalent assembly of probe ssDNA on the electrode passivates the electrode and effectively decreased the electron transfer between the redox couple in the solution and the surface of the modified electrode with a peak-

to-peak separation of 330 mV (Fig. 4(ii)). The interaction of the complementary oligonucleotides sequence (26-mer) with ssDNA/A-MWCNT/AuNPs/Ta electrode caused the decrease of the peak current of the redox couple surface (Fig. 4(iii)) with a peak-to-peak separation of 510 mV. It is because hybridization of probe ssDNA with target DNA results in the formation of increasing amounts of double-stranded DNA (ds-DNA). As a result, the charge transfer of $Fe(CN)_6^{3-}/Fe(CN)_6^{4-}$ redox reaction was further hindered.

Fig. 4

3.4. The effect of CNT density, gold nanoparticles density, and DNA probe density on sensing performance

The density of A-CNTs may influence their inherent properties, such as electron transfer rate and electrocatalytic activity and it may also influence the immobilization of biomolecule and the diffusion of substrate, which will finally influence the detecting performance of the biosensor modified with the ACNTs. The site density of the aligned CNTs can be controlled by tuning the site density of Ni nanoparticles, which serve as catalysts [31]. In order to investigate the effect of CNTs density on sensing performance, low-density aligned carbon nanotubes (LD-ACNTs) with a site density of 1×10^{9} cm^{-2} and high–density aligned carbon nanotubes (HD-ACNTs) with a site density of 1×10^{12} cm^{-2} were prepared by varying the thickness of Ni catalyst and were used to form ACNTs/Ta electrode.

The advantages of LD-ACNTs/TaE were demonstrated by comparing with HD-ACNTs/TaE in reversibility and effective surface area. Fig. 5 is the cyclic voltammograms of the electrodes modified by high (curve A) and low density (curve B) of ACNTs at scan rate of 20 mV s^{-1} in 5 mM $Fe(CN)_6^{4-/3-}$ .The peak potential difference of the LD-ACNTs/TaE electrode is about 110 mV, which is much smaller than that of the HD-ACNTs/TaE electrode (300 mV). The peak potential difference between the anodic and cathodic peak can denote the reversibility of an electrode. The smaller the peak potential difference is, the better the reversibility of the electrode is. From the peak potential difference, it can be concluded that LD-ACNTs/TaE electrode has better reversibility than the HD-ACNTs/TaE electrode. So, the electron transfer rate on LD-ACNTs/TaE is larger than that on HD-ACNTs/TaE. Also, at LD-ACNTs/TaE the redox probe reaction is significantly improved (curve B), reflected by the enlarged peak current and the decreased peak-to-peak potential separation in contrast with the HD-ACNTs/Ta electrode (curve A). The decrease of peak-to-peak potential separation in addition to enhancement in peak current sharpness and amount at this modified electrode show a strong catalytic function due to high electroactive surface areas. On the other hand, the spacing in the LD-ACNTs can make every nanotube work as an individual nanoelectrode [32], which is also contributive to the high sensitivity of the modified electrode.

Fig. 5

As expected, and in agreement with earlier reports [33,34], probe density strongly affects the target hybridization efficiency; that is, for high probe density films, we find that the efficiency of hybridization is low (Fig. 6). We prepared a series of DNA electrodes with different surface density, by varying probe concentration and self-assembly time, (see Materials and Methods). As shown in Fig. 6, DNA hybridization efficiency decreased along with the increased surface density, with highest efficiency (~80%) at low-density surfaces (1.2×10^{12} molecule/cm^2) and lowest efficiency (<5%) at high-density surfaces (1.2×10^{13} molecule/cm2). This clearly showed that control of DNA assembly was essential for sensitivity improvement, and that low-density DNA monolayers (1.2×10^{12} molecule/cm^2) were optimal for high-sensitivity DNA detection.

Fig. 6

3.5. EIS investigations at different Modified Electrodes

In this work, we used EIS as a suitable investigation technique to study the probe DNA immobilization and hybridization with the target oligonucleotides. EIS measurements were performed in presence of 5.0 mM $K_3[Fe(CN)_6]/K_4[Fe(CN)_6]$ plus 0.1 M KCl as a redox probe. Fig. 7 compares the nyquist plots of 5.0 mM $K_4Fe(CN)_6/K_3Fe(CN)_6$ at the different modified electrodes. In EIS, the semicircle part at higher frequencies corresponds to the electron transfer limited process or the electron transfer resistance. The linear part at lower frequencies results from the diffusion-limiting step of the electrochemical process (controlled-diffusion process). It is interesting that pointing out a notable difference between the EIS achieved here and those obtained with other DNA hybridization sensors is that here there are three semicircles in the EIS obtained for A-MWCNT/AuNPs/Ta modified electrodes. The first and second semicircles in Fig. 7C are likely due to the resistance of the aligned MWCNT array and Au nanoparticles. The third semicircle in EIS arises from the resistance to charge transfer from the redox probe $Fe(CN)_6^{3-}/Fe(CN)_6^{4-}$ to the ssDNA and dsDNA modified electrode surfaces and indicates the blocking behavior of the electrode surface for the redox couple. This resistance, R_{ct} (the semicircle diameter) varies by the property of the DNA film and can thus be employed as a signal to characterize the modification for each step and to determine DNA concentration in a sample.

The difference of R_{ct} was obtained based on the following equation:

$$\Delta R_{ct} = R_{dsDNA} - R_{ssDNA} \qquad (1)$$

where R_{dsDNA} is electron transfer resistance of dsDNA/A-MWCNT/AuNPs/TaE and R_{ssDNA} is electron transfer resistance of ssDNA/ A-MWCNT/AuNPs/Ta electrodes.

All the experimental impedance spectra have been fitted to an equivalent circuit model (see the inset in Fig. 10A). R_s denotes the solution resistance, i.e. a resistance between the reference and MWCNT-Au-ssDNA working electrode. The combination of R_{Au}, Q_{Au} and R_{CNT}, Q_{CNT} accounts for the behavior of MWCNT array and Au NPs. Based on the similarity with the semicircles reported in MWCNT arrays and Au nanoparticles [35, 36], here the first semicircle (i.e. R_{CNT}) is suggested to arise from vertically aligned MWCNT array and the second one (i.e. R_{Au}) arises from AuNPs resistance. Also, Q_{CNT} and Q_{Au} account for the capacitance for MWCNT and gold film. The constant phase element Q_{DNA} accounts for the capacitance of DNA film on the electrode that acts as a nonlinear capacitor accounting for the inhomogeneity of the DNA films. The semicircle related to DNA film on the electrode at higher frequencies has a higher resistance in comparison to the first and second semicircles related to A-MWCNT/AuNPs film. A Warburg impedance (W) was seen with the A-MWCNT/Au bare electrode or ssDNA/A-MWCNT/AuNPs electrode at low target DNA concentrations. The fitting also suggests that a warburg impedance is needed to achieve a good agreement between simulated and experimental EIS.

As it can be seen in Fig. 7(i), the bare Ta electrode has an enlarged R_{ct} (334 kΩ) which upon the modification of Ta electrode with aligned MWCNTs, a significant decrease in R_{ct} to 14 kΩ can be observed (Fig. 7(ii)). In fact binding of A-MWCNTs on the electrode surface generated a conducting porous layer on the electrode surface that functioned as a promoter to the interfacial electron transfer. Noticeably, when the AuNPs were electrodeposited onto the aligned MWCNTs surface, R_{ct} decreased dramatically to 4 kΩ (Fig. 7(iii)).The lower R_{ct} indicated that the A-

MWCNTs/AuNPs/Ta modified electrode possessed an excellent conductive interface and the results could be rationalized by improved electron transfer kinetics of redox probe on A-MWCNTs/AuNPs modified electrode. All these data show that the stepwise modified material, was successfully assembled on the Ta electrode surface and formed a tunable kinetic promoter. Immobilization of probe ssDNA onto the surface of A-MWCNT/AuNPs/Ta electrode leads to an increase in the electron transfer resistance (8.5 kΩ). It is because the self-assembled monolayer of ssDNA acts as an insulating layer, which hinders the interfacial electron transfer of $Fe(CN)_6^{3-}/Fe(CN)_6^{4-}$ at the electrode surface due to electrostatic interactions. Indeed, the strong electrostatic repulsion between the $K_4Fe(CN)_6/K_3Fe(CN)_6$ molecules and the negative-charged phosphate skeletons of ssDNA results in an obvious increase in R_{ct} (Fig. 7(iv)). After hybridization of the probe DNA with 2.0×10^{-7} M complementary DNA, R_{ct} was obviously increased to 11 kΩ (Fig. 7(v)). This phenomenon is due to the generation of an insulating layer on the modified electrode surface, which results in a higher electron transfer resistance and significantly enlarges the diameter of the semicircle. Hybridization of probe ssDNA with target DNA results in the formation of increasing amounts of double-stranded DNA (ds-DNA).ds-DNA subsequently enhances the electrostatic interaction between the redox marker and the backbone of the oligonucleotide. As a result, the charge transfer of $Fe(CN)_6^{3-}/Fe(CN)_6^{4-}$ redox reaction was further hindered. The results obtained from EIS measurements (Fig. 7) are in good agreement with the results extracted from cyclic voltammograms (Fig. 4) and confirm the successful immobilization of ssDNA on the surface of A-MWCNT/AuNPs/Ta electrode. Therefore, this impedance change indicated that modification and DNA hybridization successfully occurred on the electrode surface.

Fig. 7

3.6. Optimization of DNA Assay Conditions

The influence of experimental variables including the time of hybridization, and hybridization temperature were studied to find the optimum conditions. The effect of hybridization time on ΔR_{ct} signals was investigated. For achieving this, the ssDNA sensor was immersed into the target solution containing 2.0×10^{-7} M target DNA at room temperature for different times of 30, 60, 90, 120 and 150 min (Fig. 8). The results indicated that by increasing the contact time between the ssDNA sensor and the target DNA, the interaction between the probe and the complementary DNA increased to 120 min, and then the signal (ΔR_{ct}) was leveled off. Therefore, a hybridization time of 120 min was selected for further study, in which the interaction between ssDNA and target DNA was maximized.

Fig. 8

Fig. 9 shows the nyquist plot of the ssDNA/A-MWCNT/AuNPs/Ta electrode (curve 1), whereas curves (2–7) of Fig. 9 show nyquist plots after hybridization of the probe DNA with the complementary oligonucleotides sequence (2.0×10^{-7} M) at different temperatures. As it could be seen, when the hybridization occurred, the electron transfer resistance increased. This is because the repulsive interaction increased between the negatively charged interface and anionic redox probe (when dsDNA was formed on the electrode) similar to the literature [37,38]. It is obvious that ΔR_{ct} was the largest at 42 ^{o}C, indicating that 42 ^{o}C was the most suitable temperature for the hybridization reaction. The results showed that the hybridization efficiency was maximized at this temperature. Thus, an optimum temperature value of 42 ^{o}C was chosen.

Fig. 9

3.7. Figures of merit and electrochemical DNA Analytical Performance

Under the optimal conditions, the analytical performance of the DNA biosensor was investigated by using the immobilized probe DNA to be hybridized by the different concentrations of the complementary sequence. When the ssDNA/A-MWCNT/AuNPs/Ta electrode was employed to measure complimentary DNA solution, increasing R_{ct} was obtained in respect to the increase of target DNA concentration (see EIS curves 2 to 9 in Fig. 10A). As it was mentioned, it is because hybridization of probe ssDNA with target DNA results in the formation of increasing amounts of double-stranded DNA (ds-DNA), which subsequently enhances the electrostatic interaction between the redox marker and the backbone of the oligonucleotide. As a result, the charge transfer of $Fe(CN)_6^{3-}/Fe(CN)_6^{4-}$ redox reaction was further hindered. The difference between the R_{ct} value of 5.0 mM $K_3[Fe(CN)_6]/K_4[Fe(CN)_6]$ at the surface of ssDNA/A-MWCNT/AuNPs/TaE and the one at the hybridization-modified electrode (dsDNA/A-MWCNT/AuNPs/TaE) were used as the measurement signal to determine the sequence specific DNA related to the *TP53* gene fragment. The results are shown in Fig. 8. The plot of the difference values of ΔR_{ct} versus the logarithm of the *TP53* gene fragment concentration (Fig. 10B) showed a good straight line, with the regression equation ΔR_{ct} (ohm) = 1417 log C + 21290 (R^2=0.997, C: $molL^{-1}$) for 1.0×10^{-15}–1.0×10^{-7} M of *TP53* gene. In this regard, three replicate measurements were done for each concentration of target DNA. The EIS measurements illustrate that a detectable increase in the charge transfer resistance could be attained for the target DNA concentration as low as 1.0×10^{-17} M. In other words, the actual lowest experimentally detected concentration (LOD) for the 26-mer complementary oligonucleotides was 1.0×10^{-17} M (S/N=3). The limit of detection has been defined as three times the standard deviation of the blank sample measurements (signal/noise of 3 (S/N=3) between the detection signal of low concentration samples and the noise of blank samples, n=11). This detection limit is much lower than previously reported works [8-10,41,42] describing an excellent performance and enhanced electrocatalytic effects of A-MWCNT/AuNPs/Ta modified electrode in detection of the *TP53* gene mutation. These results are comparable with other's works as Table 1 illustrated. As it can be seen, the prepared biosensor had a large linear range and lower detection limit than other current TP53 electrochemically based biosensors, indicating the feasibility and the superiority of the DNA biosensor which was reliable for the detection of the *TP53* gene mutation at low concentrations. So these results indicated that the proposed electrode is sensitive, rapid, and considerably simpler than traditional ones for *TP53* gene mutation detection due to the integration of Au nanoparticles and aligned MWCNTs which represents a promising platform for achieving sensitive biosensor for fast mutation screening related to most human cancer types.

Fig. 10

Table1

3.8. Selectivity, reproducibility, reusability, and stability of the biosensor

The selectivity of this ssDNA/A-MWCNT/AuNPs/Ta electrode was examined in Fig. 11 (A,B), where responses to ssDNA/A-MWCNT/AuNPs bare electrode, 1-base mismatched, 3-base mismatched and complimentary DNAs were depicted. Fig. 11 (A) shows nyquist plots for ssDNA/A-MWCNT/AuNPs/TaE electrodes hybridized with 0 M (curve 1), 1 pM 3-base

mismatched (curve 2) , 1 pM 1-base mismatched (curve 3), and 1 pM complimentary target DNAs (curve 4). Fig. 11(B) also represents the ΔR_{ct} measured at ssDNA/A-MWCNT/AuNPs/Ta electrodes hybridized with the same DNAs as mentioned in Fig. 11 (A).

As it can be seen in Fig. 11 (A,B), a single nucleotide mismatch introduced disorder into the ds-DNA film, weakening the interaction between the redox probe and ds-DNA. It consequently allowed the redox probe to penetrate into the film to a larger extent. As a result, the R_{ct} value was reduced in comparison with ssDNA/A-MWCNT/AuNPs bare electrode (Fig. 11 (A,B) curve 3) . For 3-base mismatched target DNAs, more disorders were introduced into the ds-DNA film, and the R_{ct} became nearly the same as that of ssDNA/A-MWCNT/AuNPs bare electrode (Fig. 11(A,B) curve 2). The great R_{ct} difference between complimentary and 1-base mismatched target DNA illustrates that the functionalized MWCNT-Au platform is highly selective. The selectivity remains even at the target DNA concentration as low as 1 pM (Fig. 11 (A,B) curve 4).

Fig. 11

Reusability of DNA biosensor is a key factor in their application and development. The reusability of above ssDNA/A-MWCNT/AuNPs/Ta electrode was analyzed via measuring against 1.0×10^{-12} M complimentary DNAs. After each measurement, the electrode was regenerated upon dehybridization in hot water (80 ^{0}C) for 5 min, which completely removed hybridized DNA via thermal denaturation [39, 40]. After each cycle, R_{ct} of the ssDNA/A-MWCNT/AuNPs/Ta electrode was found to increase slightly. Also, the obtained R_{ct} of 1.0×10^{-12} M complimentary DNA increases slightly after every dehybridization (<1%) (Fig. 12). The results showed that the 4th regenerated sensor had 93.4% EIS response of the initial electrode, which indicated that the proposed DNA biosensor had a good reusability.

Fig.12

The stability of the biosensor was also examined. When the biosensor was stored in the refrigerator at 4 ^{o}C and measured intermittently (every 7 days), it retained about 91.6% of its original response after 2 weeks, indicating that the modified electrode was stable. The reproducibility of biosensor is a very important factor for their application. Five DNA sensors were fabricated independently under the same conditions and used to detect 2.0×10^{-7} M complementary DNA. Relative standard deviation (RSD) was 2.1% which indicated a suitable reproducibility of the proposed biosensor.

Conclusion:

For the first time, this study prepared a new platform for lable-free DNA detection of the *TP53* gene mutation, one of the most popular genes in cancer research, which is based on electrochemical growth of Au NPs on vertically aligned MWCNT array. Using EIS, over the extended DNA concentration range, the change of charge transfer resistance was found to have a linear relationship in respect to the logarithm of the complementary oligonucleotides sequence concentrations at the low concentration range of 1.0×10^{-15}–1.0×10^{-7} M, with a detection limit of 1.0×10^{-17} M (with a signal-to-noise of 3), which is lower than any reported results so far. The high selectivity of the ssDNA/A-MWCNT/AuNPs electrode was examined and results showed that this nanosensor can effectively distinguish between the one-base mismatched oligonucleotides sequence and the noncomplementary oligonucleotides sequence with complementary oligonucleotides sequence, and it has a higher sensitivity to detect the complementary oligonucleotides sequence at an ultra-trace level. The simple manipulation procedure, low cost, fast response, high sensitivity and a broad linear range are the main features of the proposed DNA sensor. In addition, by direct growth of A-MWCNTs on Ta, individual nanotubes are electrically connected to the conductive acid-resisting substrate which promotes

further more electron transfer reaction. The significant improvement of this platform over those utilizing alone MWCNT or Au NPs indicates synergistic interactions of aligned MWCNT array and Au NPs. When those aligned MWCNT were replaced by random MWCNT matrix, changing the R_{ct} decreases, unveiling the unique advantages of vertically aligned MWCNT array electrodes as a new platform in biosensing.

References:

[1] N. Falette, M.P. Paperin, I. Treilleux, A.C. Gratadour, N. Peloux, H. Mignotte, et al. Prognostic value of p53 gene mutations in a large series of node-negative breast cancer patients, Cancer Res. 58 (1998) 1451–1455.

[2] D.R. Walker, J.P. Bond, R.E. Tarone, C.C. Harris, W. Makalowski, M.S. Boguski, et al., Evolutionary conservation and somatic mutation hotspots maps of p53: correlation with p53 protein structural and functional features, Oncogene 19 (1999) 211–218.

1 [3] S. Razin, DNA probes and PCR in diagnosis of mycoplasma infections, Mol. Cell. Probes 8 (1994) 497-511.

[4] T. Jiang, M. Minunni, M. Mascini, Towards fast and inexpensive molecular diagnostic: the case of p53, Clin. Chim. Acta 343 (2004) 45–60.

[5] P. Nilsson, B. Persson, A. Larsson, M. Uhlen, P.A. Nygren, Detection of mutations in PCR products from clinical samples by surface plasmon resonance, J Mol Recogn. 10 (1) (1997) 7–17.

[6] P. Nilsson, A. Larsson, J. Lundeberg, M. Uhlen, P.A. Nygren, Mutational scanning of PCR products by subtractive oligonucleotide hybridization analysis, Biotechniques 26 (2) (1999) 308–316.
[7] T. Jiang, M. Minunni, P. Wilson, J. Zhang, A.P.F Turner, M. Mascini, Detection of TP53 mutation by a portable surface plasmon resonance biosensor, Biosens. Bioelectron. 20 (10) (2005) 1939–1954.
[8] J. Wang, P.E. Nielsen, M. Jiang, X. Cai, J. Fernandes, D. Grant, et al., Mismatch sensitive Hybridization detection by peptide nucleic acids immobilized on a quartz crystal microbalance, Anal. Chem. 69 (1997) 5200–5202.
[9] J. Wang, G. Rivas, X. Cai, M. Chicharro, C. Parrado, N. Dontha, et al., Detection of point mutation in the p53 gene using a peptide nucleic acid biosensor, Anal. Chim. Acta 344 (1997) 111–118.
[10] H. Miyahara, K. Yamashita, M. Kanai, K. Uchida, M. Takagi, H. Kondo, et al., Electrochemical analysis of single nucleotide polymorphisms of p53 gene, Talanta 56 (2002) 829–835.
[11] T.G. Drummond, M.G. Hill, J.K. Barton, Electrochemical DNA sensors, Nat. Biotechnol. 21 (2003)1192–1199.
[12] , P.G. He, L.M. Dai, Aligned carbon nanotube-DNA electrochemical biosensors, Chem. Commun. 3 (2004) 348–349.
[13] R.J. Chen, S. Bangsaruntip, K.A. Drouvalakis, S.K. Wong, M. Shim, Y. Li, W. Kim, P.J. Utz, H. Dai, Proc. Natl. Acad. Sci. U.S.A. 100 (2003) 4984–4989.
[14] X.Z. Zhang, K. Jiao, S.F. Liu, Y.W. Hu, Readily reusable electrochemical DNA hybridization biosensor based on the interaction of DNA with single-walled carbon nanotubes, Anal. Chem. 81 (2009) 6006–6012.
[15] H. Pei, N. Lu, Y. Wen, S. Song, Y. Liu, H.C. Yan Fan, A DNA Nanostructure-based Biomolecular Probe Carrier Platform for Electrochemical Biosensing, Adv. Mater. 22 (2010) 4754–4758.
[16] X. Tang, S. Bansaruntip, N. Nakayama, E. Yenilmez, Y. Chang, Q. Wang, Carbon Nanotube DNA Sensor and Sensing Mechanism, Nano Lett. 6 (2006) 1632–1636.
[17] Y. Weizmann, D.M. Chenoweth, T.M. Swager, DNA-CNT Nanowire Networks for DNA Detection, J. Am. Chem. Soc. 133 (2011) 3238–3241.
[18] K. Pinwattana, J. Wang, C.T. Lin, H. Wu, D. Du, Y.H. Lin, O. Chailapakul, CdSe/ZnS quantum dots based electrochemical immunoassay for the detection of phosphorylated bovine serum albumin, Biosens. Bioelectron. 26 (2010) 1109–1113.
[19] W.S. Lu, L. Lin, L. Jiang, Nanogold hollow balls with dendritic surface for hybridization of DNA, Biosens. Bioelectron. 22 (2007) 1101–1105.
[20] Y. Xu, H. Cai, , P.G. He, Y.Z. Fang, Probing DNA Hybridization by Impedance Measurement Based on CdS-Oligonucleotide Nanoconjugates, Electroanalysis 16 (2004) 150–155.
[21] X.X. Li, L.H. Shen, D.D. Zhang, H.L. Qi, Q. Gao, F. Ma, C.X. Zhang, Electrochemical impedance spectroscopy for study of aptamer–thrombin interfacial interactions, Biosens. Bioelectron. 23 (2008) 1624–1630.
[22] P. J. F. Harris, Carbon Nanotubes and Related Structures—New Materials for the Twenty-First Century, Cambridge University Press: Cambridge, 2001.
[23] B.R. Azamian, J. J. Davis, K. S. Coleman, C. B. Bagshaw, M. L. H. Bioelectrochemical Single-Walled Carbon Nanotubes, J. Am. Chem. Soc. 124 (2002) 12664-12665.

[24] J. Li, H.T. Ng, A. Cassell, W. Fan, H. Chen, Q. Ye, J. Koehne, J. Han, M. Meyyappan, Carbon Nanotube Nanoelectrode Array for Ultrasensitive DNA Detection, Nano Lett. 3 (2003) 597-602.
[25] L.Q. Chu, W. Knoll, R. Förch, Plasma polymerized epoxide functional surfaces for DNA probe immobilization, Biosens. Bioelectron. 24 (2008) 118-122.
[26] Y. Xu, H. Cai, P.G. He, Y.Z. Fang, Probing DNA Hybridization by Impedance Measurement Based on CdS-Oligonucleotide Nanoconjugates, Electroanalysis 16 (2004) 150-155.
[27] H.H. Huang, J. Zhou, Y.P. Huang, J.L. Kong, Impedimetric immunosensor with on-chip integrated electrodes for high-throughput screening of liver fibrosis markers, J. Anal. Chem. 63 (2008) 492-498.
[28] B. Rezaei, T. Khayamian, N. Majidi, H. Rahmani, Immobilization of specific monoclonal antibody on Au nanoparticles for hGH detection by electrochemical impedance spectroscopy, Biosens. Bioelectron. 25 (2009) 395-399.
[29] J.Y. Park, S.M. Park, DNA Hybridization Sensors Based on Electrochemical Impedance Spectroscopy as a Detection Tool, Sensors 9 (2009) 9513–9532.
[30] A. Dolati, M. Ghorbani, M.R. Ahmadi, An electrochemical study of Au–Ni alloy electrodeposition from cyanide–citrate electrolytes, J. Electroanal. Chem. 577 (2005) 1-8.
[31] B. Yue, Y.W. Ma, H.S. Tao, L.S. Yu, G.Q. Jian, X.Z. Wang, X.S. Wang, Y.N. Lu, Z. Hu, CNx nanotubes as catalyst support to immobilize platinum nanoparticles for methanol oxidation, J. Mater. Chem. 18 (2008) 1747–1750.
[32] Y. Tu, Z.P. Huang, D.Z. Wang, J.G. Wen, Z.F. Ren, Growth of aligned carbon nanotubes with controlled site density, Appl. Phys. Lett. 80 (2002) 4018–4020.
[33] A.B. Steel, T.M. Herne, M.J. Tarlov, Electrochemical quantitation of DNA immobilized on gold, Anal. Chem. 70 (1998) 4670-4677.
[34] E. Huang, M. Satjapipat, S. B. Han, F.M. Zhou, surface structure and coverage of an oligonucleotide probe tethered onto a gold substrate and its hybridization efficiency for a polynucleotide target, Langmuir, 17 (2001) 1215-1224.
[35] Y. Zhang, Z.Wang, Y.Wang, L. Huang,W. Jiang, M.Wang, Electrochemical Detection of Sequence-Specific DNA with the Amplification of Gold Nanoparticles, Int. J. Electrochemi. 2012 (2011) 1-7.
[36] A. Bonannia, M. del Valle, Use of nanomaterials for impedimetric DNA sensors: A review, Anal. Chim. Acta 678 (2010) 7–17.
[37] Y. Huang, M.C. Bell, I.I. Suni, Impedance Biosensor for Peanut Protein Ara h 1, Anal. Chem. 80 (2008) 9157-9161.
[38] K. Zhang, H. Ma, L. Zhang, Y. Zhang, Fabrication of a sensitive impedance biosensor of DNA hybridization based on gold nanoparticles modified gold electrode, Electroanalysis 20 (2008) 2127-2131.
[39] D.L. Li, X.Q. Zou, Q. Shen, S.J. Dong, Kinetic study of DNA/DNA hybridization with electrochemical impedance spectroscopy, Electrochem. Commun. 9 (2007) 191–196.
[40] J. Zhang, S.P. Song, L.Y. Zhang, L.H. Wang, H.P. Wu, D. Pan, C.H. Fan, Sequence-Specific Detection of Femtomolar DNA via a Chronocoulometric DNA Sensor (CDS): Effects of Nanoparticle-Mediated Amplification and Nanoscale Control of DNA Assembly at Electrodes, J. Am. Chem. Soc. 128 (2006) 8575-8580.
[41] E. Hamidi-Asl, I. Palchetti, M. Mascini, Introduction of an Electrochemical Genosensor for Detection of P53 Gene Via Sandwich Hybridization Method, A. D'Amico et al. (eds.), Sensors

and Microsystems: AISEM 2011 Proceedings, Lecture Notes in Electrical Engineering 109, DOI 10.1007/978-1-4614-0935-9_7, # Springer Science+Business Media, LLC 2012.
[42] J. B. Raoof, R. Ojani, S. M. Golabi, E. Hamidi-Asl, M. S. Hejazi, Preparation of an electrochemical PNA biosensor for detection of target DNA sequence and single nucleotide mutation on p53 tumor suppressor gene corresponding oligonucleotide, Sensors and Actuators B 157 (2011) 195– 20.

Scheme 1. Schematic representations of the DNA electrochemical biosensor.

Fig. 1 (A,B) SEM images of well aligned CNTs grown on the polished Ta substrate at 850 ^{0}C after 6 minutes shown with different resolutions. (C,D) TEM images of bamboo-like structure of multi-walled CNTs with different resolutions.

Fig. 2 (A) chronoamperometry curve of the deposited AuNPs on the CNTs at potential of +0.2 V after 10 s in 0.5 M H_2SO_4 containing 5 mM $HAuCl_4$ (B) SEM image of the deposited AuNPs on the CNTs using chronoamperometry at the mentioned condition, (C) SEM image of AuNPs on A-CNTs at the same condition with keeping the alignment from the side view.

Fig. 3. Cyclic voltammograms of i) bare Ta electrode, ii) entangled-MWCNT/Ta electrode, iii) aligned-MWCNT/Ta modified electrode and iv) A-MWCNT/AuNPs/Ta modified electrode; conditions: 5.0 mM $K_4Fe(CN)_6$/ $K_3Fe(CN)_6$, and 0.1 M KCl with scan rate of 5 mV s^{-1}.

Fig. 4 cyclic voltammograms of i) A-MWCNT/AuNPs/Ta electrode, ii) ssDNA/A-MWCNT/AuNps/Ta electrode, iii) ssDNA/A-MWCNT/AuNps/TaE after hybridized with 26-mer target DNA (2×10^{-7}M); Conditions: 5.0 mM $K_4Fe(CN)_6$/ $K_3Fe(CN)_6$ and 0.1 M KCl with scan rate of 5 mV s^{-1}.

Fig. 5 Cyclic voltammograms of A) HD-ACNTs/Ta electrode, B) LDACNTs/ Ta-modified electrode in 5.0 mM $K_4Fe(CN)_6$/$K_3Fe(CN)_6$, with scan rate of 20 mV s^{-1}

Fig. 6 Comparison of hybridization efficiency for A-MWCNTs/AuNps/Ta electrodes with different DNA surface density. Error bars show the standard deviations of measurements taken from at least three independent experiments. L, M, and H stand for low-density (1.2×10^{12} molecule/cm^2), medium-density (6×10^{12} molecule/cm^2), and high-density (1.2×10^{13} molecule/cm^2) surfaces.

Fig. 7 Nyquist plot of different electrodes immersed into 2.0×10^{-7} M 26-mer target DNA for 120 min at 42 ^{o}C: (i) bare Ta electrode ; (ii) A-MWCNT/Ta electrode;
(iii) A-MWCNT/AuNPs/Ta electrode; (iv) ssDNA/A-MWCNT/AuNPs/Ta modified electrode;
(v) dsDNA/A-MWCNT/AuNPs/TaE.

Fig. 8 Nyquist plot of the ssDNA/A-MWCNT/AuNPs/Ta electrode immersed into 2.0×10^{-7} M DNA target for in 42^{o}C in different times; (a) hybridization at 30 min; (b) hybridization at 60 min; (c) hybridization at 90 min; (d) hybridization at 120 min; and (e) hybridization at 150 min.

Fig. 9. Nyquist plot of the ssDNA/A-MWCNT/AuNPs/Ta electrode immersed into 2.0 $\times 10^{-7}$ M 26-mer DNA target for 120 min in different temperature; (a) the probe; (b) hybridization at 25 ^{o}C; (c) hybridization at 32 ^{o}C; (d) hybridization at 35 ^{o}C; (e) hybridization at 42 ^{o}C; (f) hybridization at 45 ^{o}C; and (g) hybridization at 50 ^{o}C.

Fig. 10 (A) Nyquist plots for ssDNA/A-MWCNT/AuNPs/Ta electrodes hybridized with the following amounts of complimentary DNA: (1) 0, (2)1.0×10^{-15} M, (3) 5.0×10^{-15} M, (4) 1.0×10^{-12} M, (5) 1.0×10^{-11} M, (6) 1.0×10^{-10} M, (7) 1.0×10^{-9} M, (8) 1.0×10^{-8} M, and (9) 1.0×10^{-7}. The inset shows the equivalent circuit of the EIS responses. (B) Plot of ΔR_{ct} vs the concentration of target DNA. Conditions: treated time 90 min, hybridization temperature 42 ^{0}C in 5.0 mM $K_4Fe(CN)_6$/ $K_3Fe(CN)_6$ and 0.1 M KCl solution.

Fig. 11 (A) Nyquist plots for ssDNA/A-MWCNT/AuNPs/TaE electrodes hybridized with (1) 0 M, (2) 1 pM 3-base mismatched , (3) 1 pM 1-base mismatched, and (4) 1 pM complimentary target DNAs; (B) ΔR_{ct} measured at ssDNA/A-MWCNT/AuNPs/Ta electrodes hybridized with the same DNAs as mentioned in part (A) .

Fig. 12. R_{ct} achieved with a DNA functionalized A-MWCNT/AuNPs electrode: (ssDNA) nonhybridized and (dsDNA) hybridized with 1.0×10^{-12} M complimentary DNA.

731 Fig. 1
732

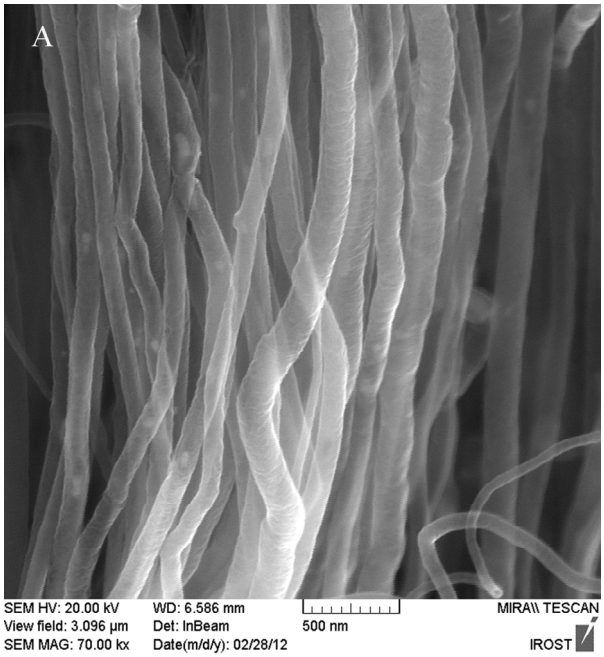

733

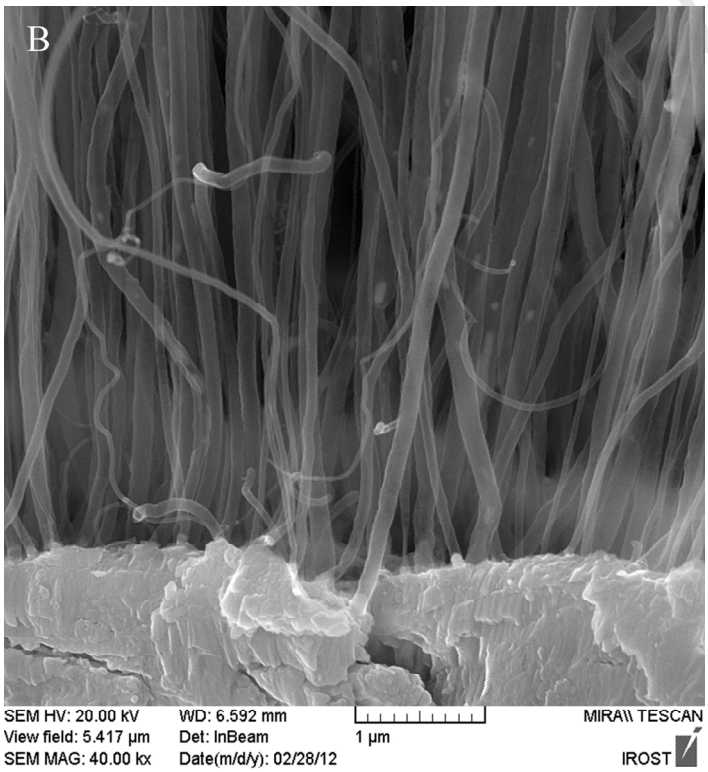

734
735
736
737

738

739
740
741

742

743 Fig. 2
744

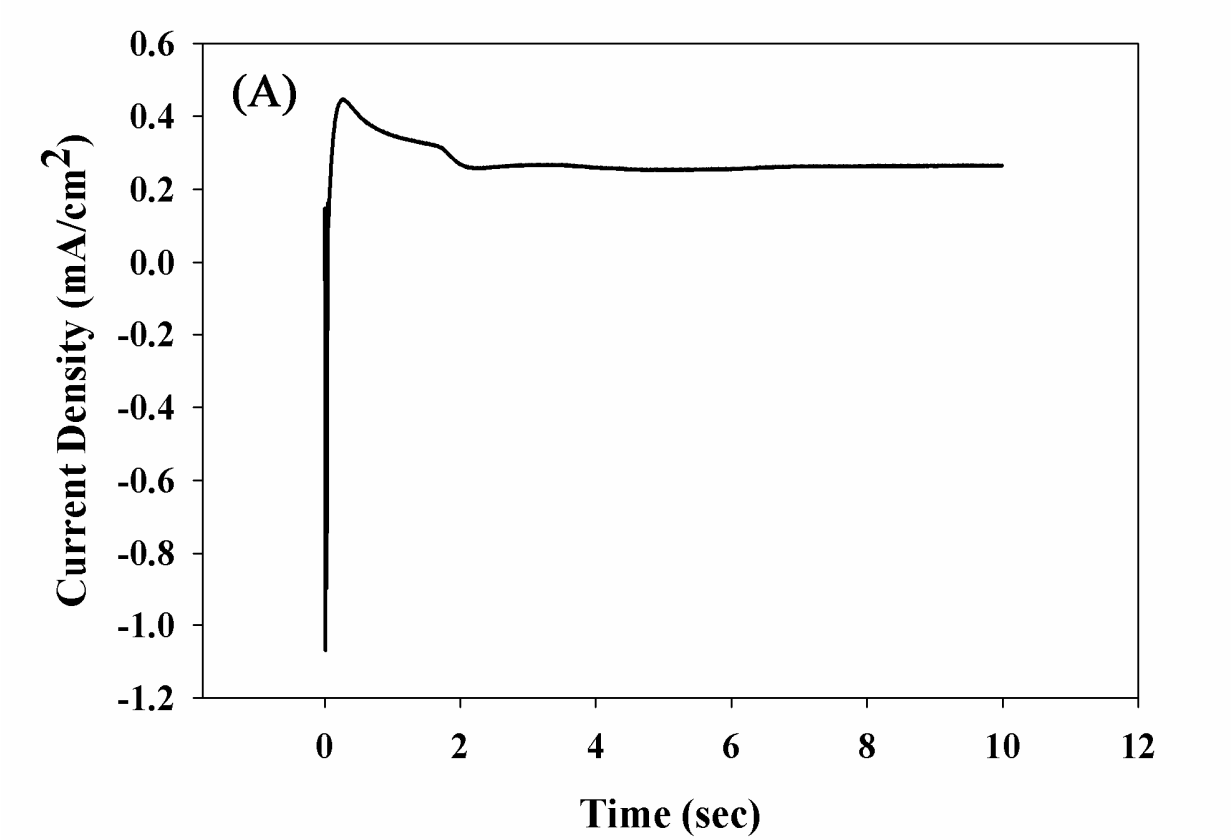

745
746

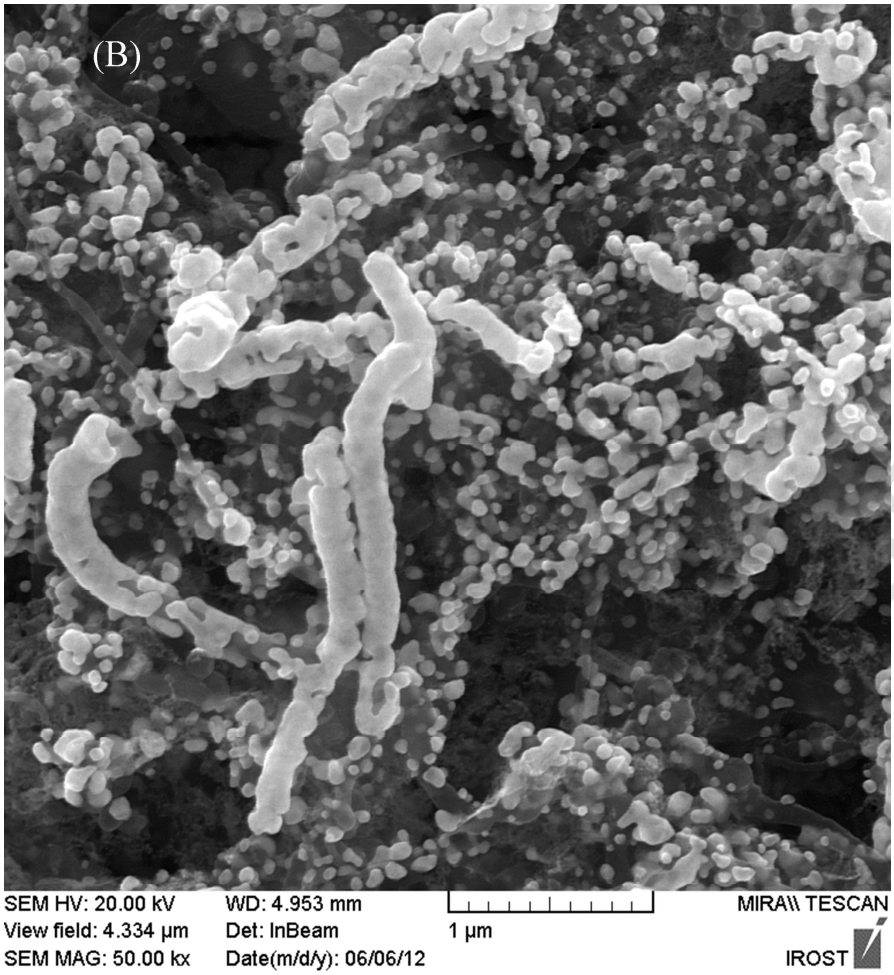

747

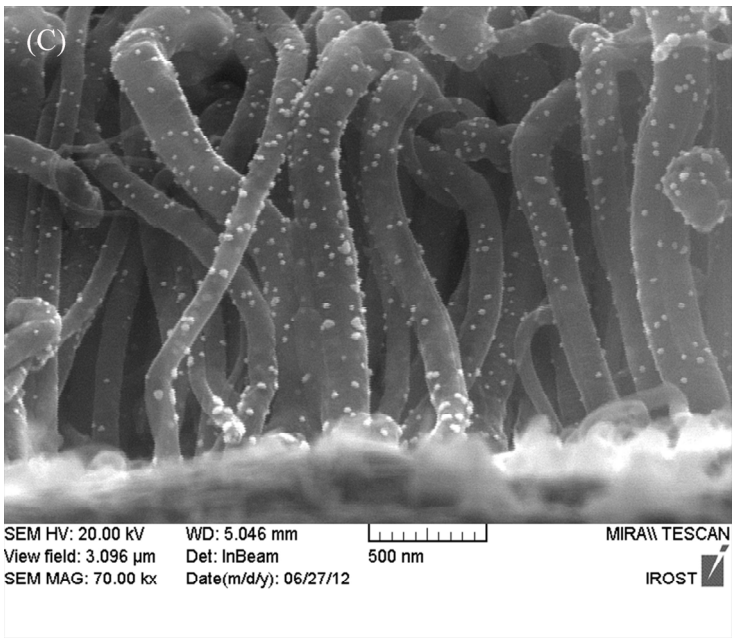

748

749 Fig. 3
750

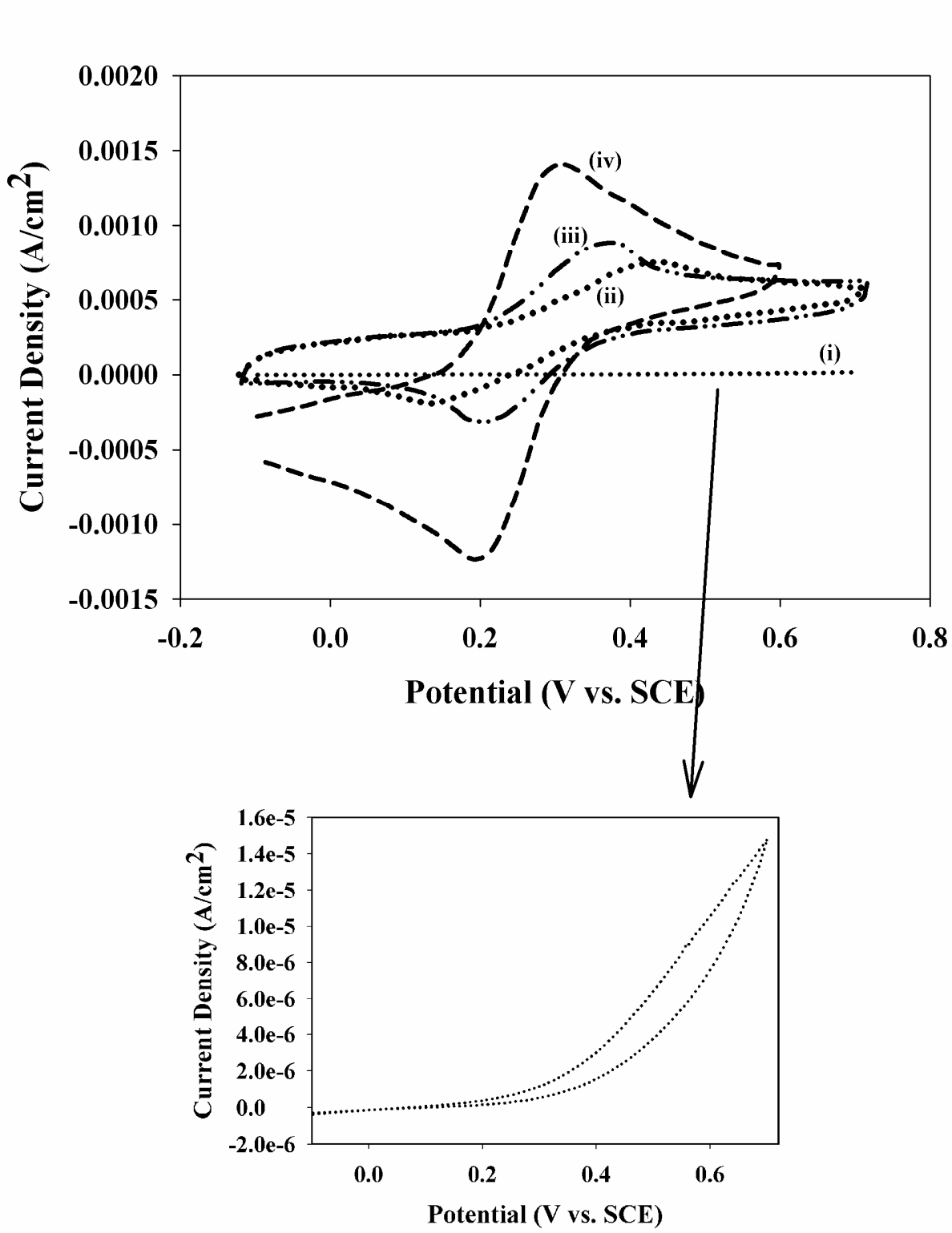

751

752 Fig. 4

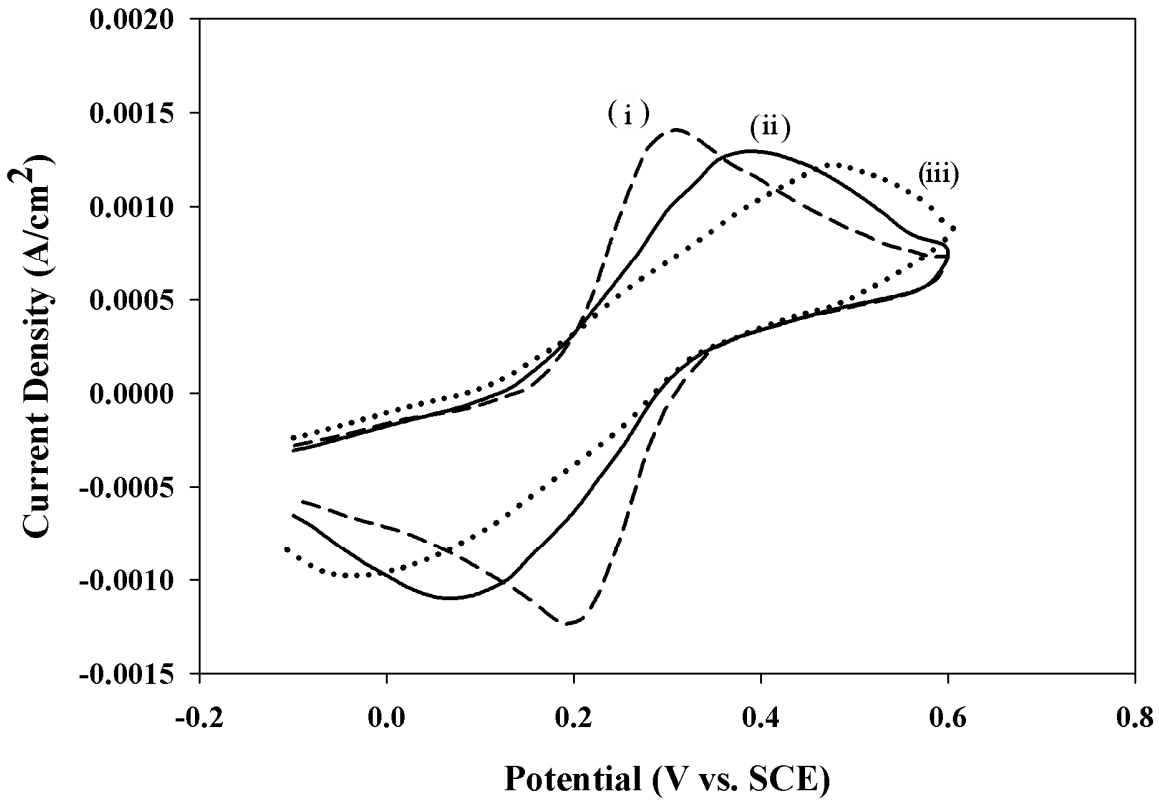

753
754
755
756 Fig.5
757

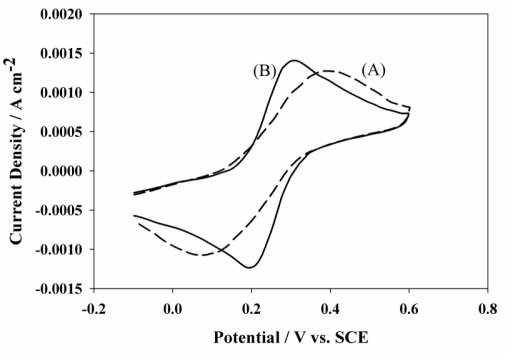

758
759
760
761
762
763
764
765

Fig. 6

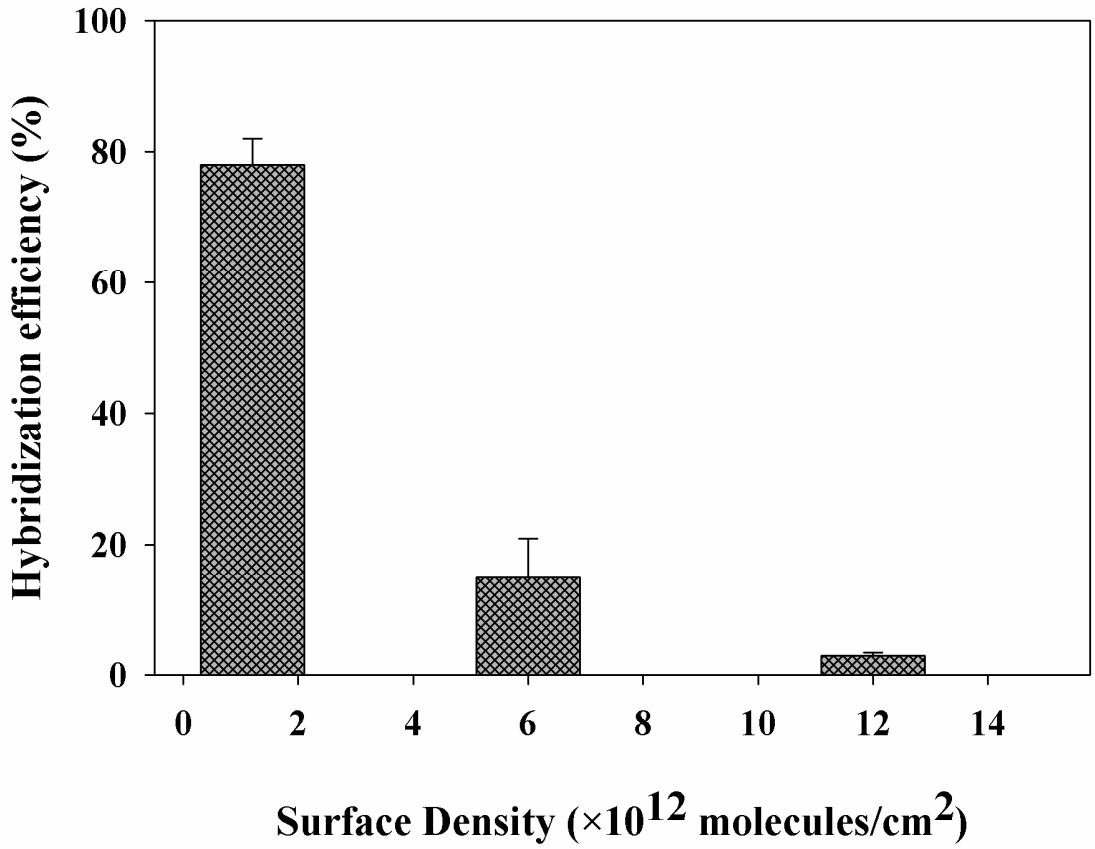

Fig. 7

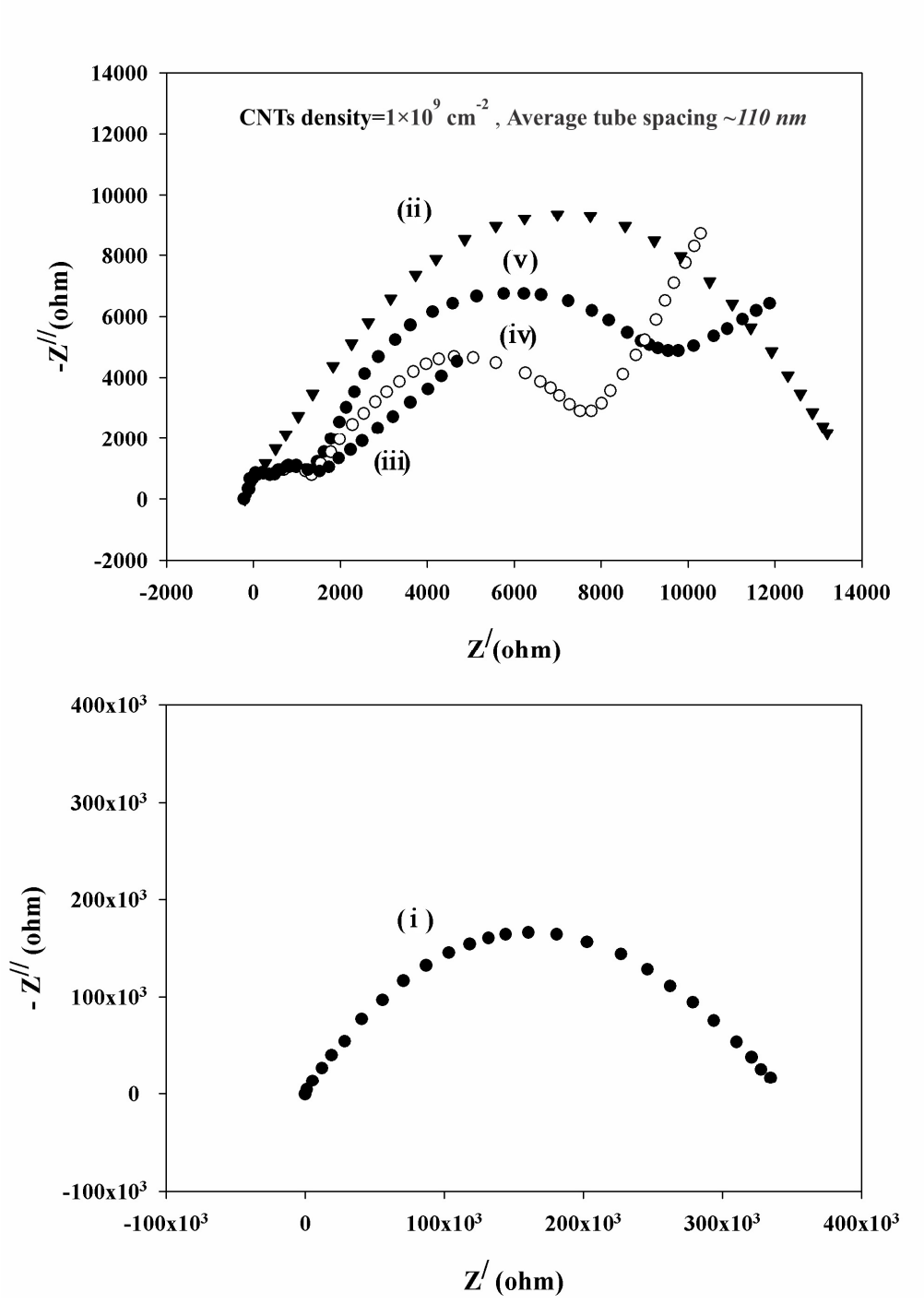

796
797 Fig.8
798

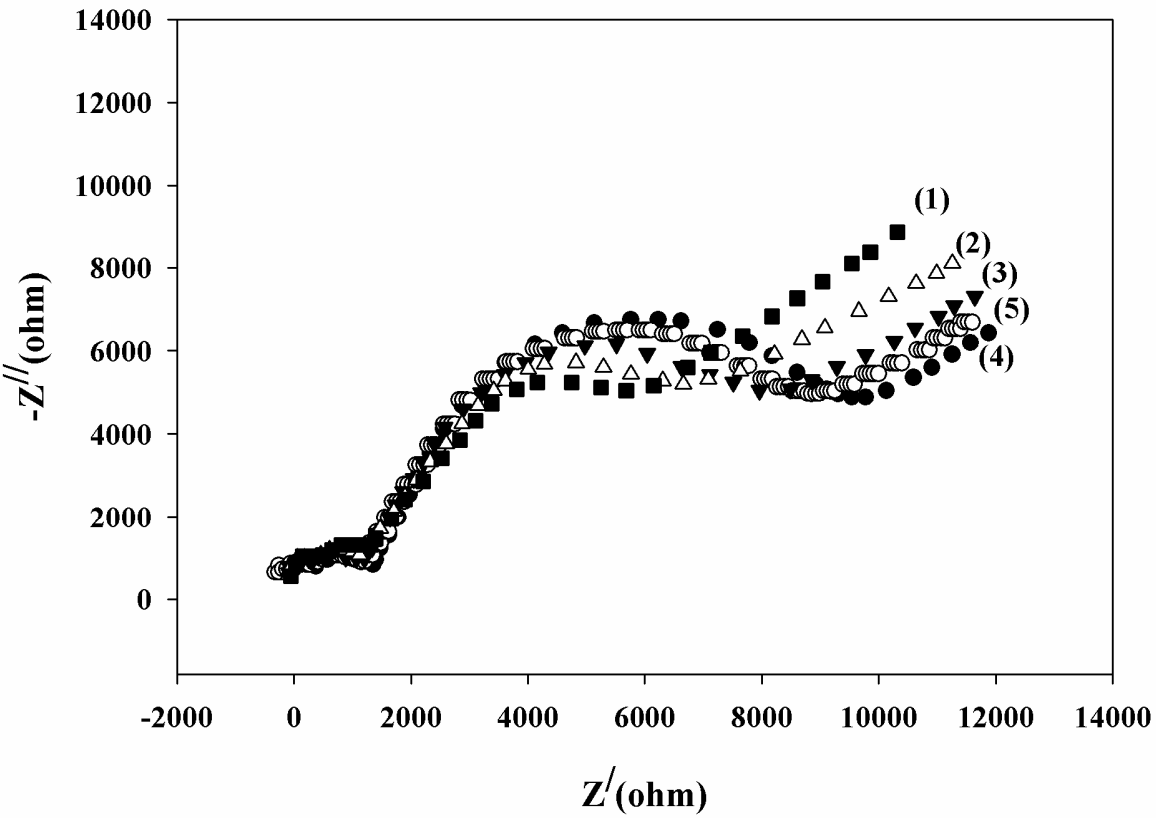

799
800 Fig. 9
801

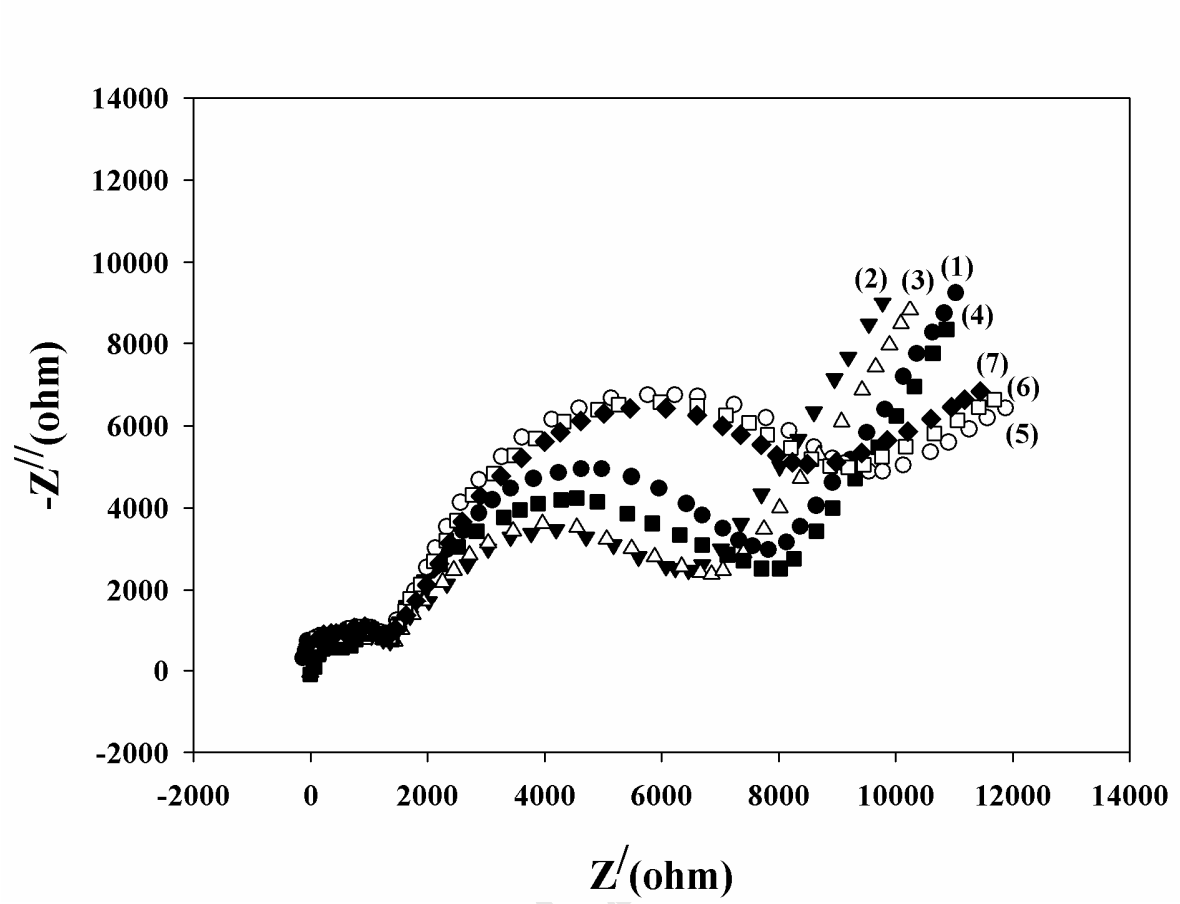

824
825 Fig.10

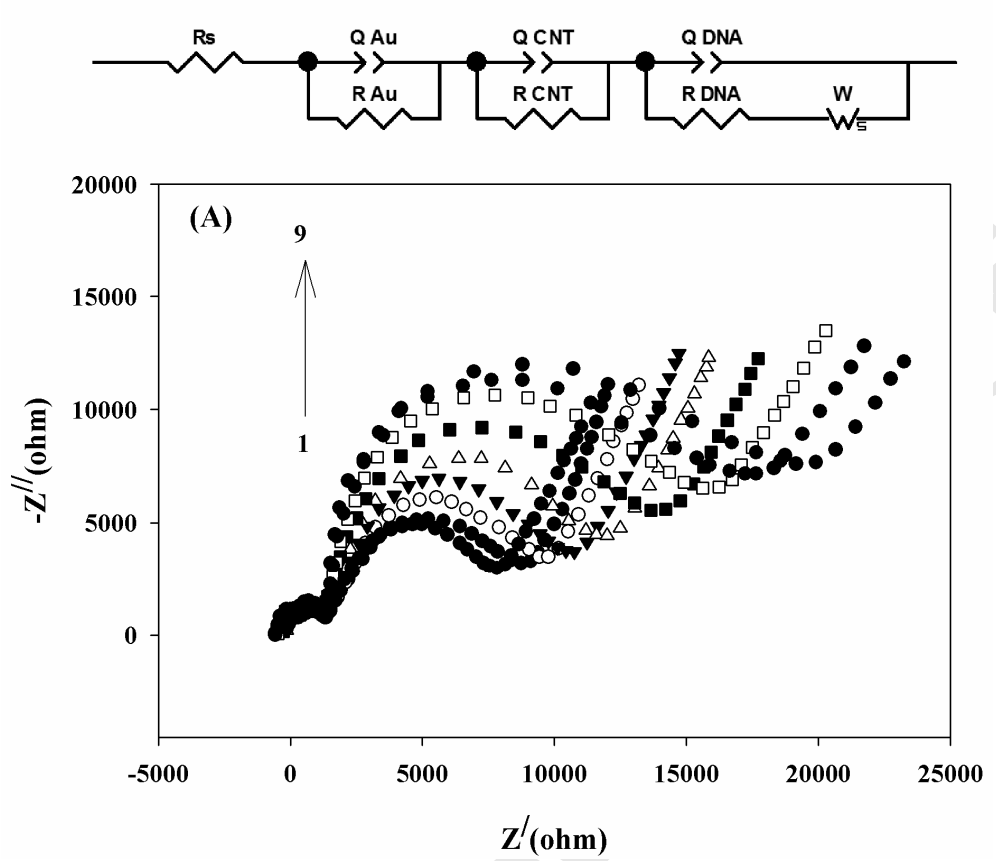

826
827

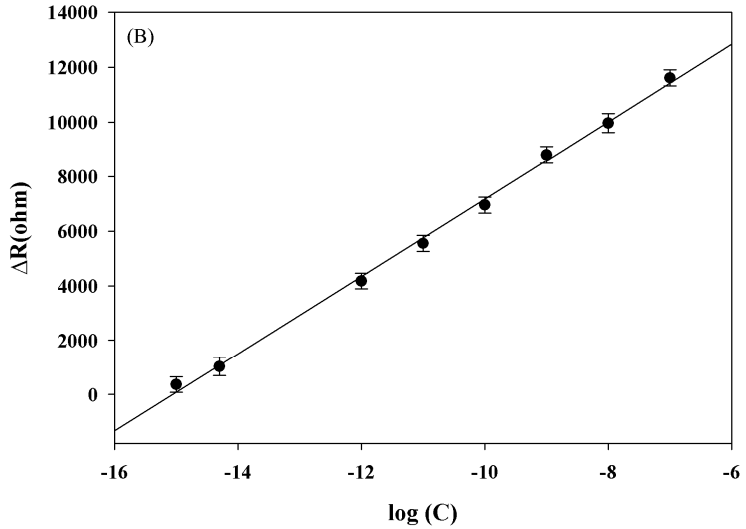

828
829
830
831

832 Fig.11

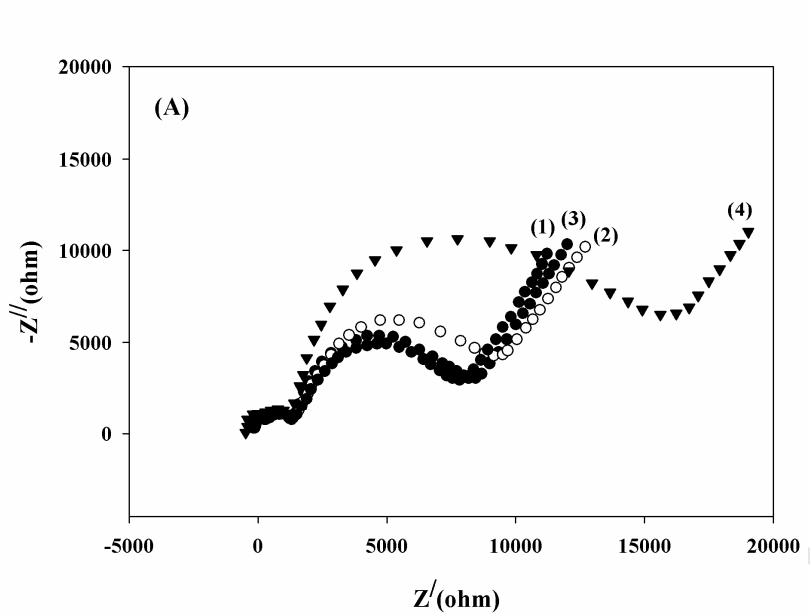

833

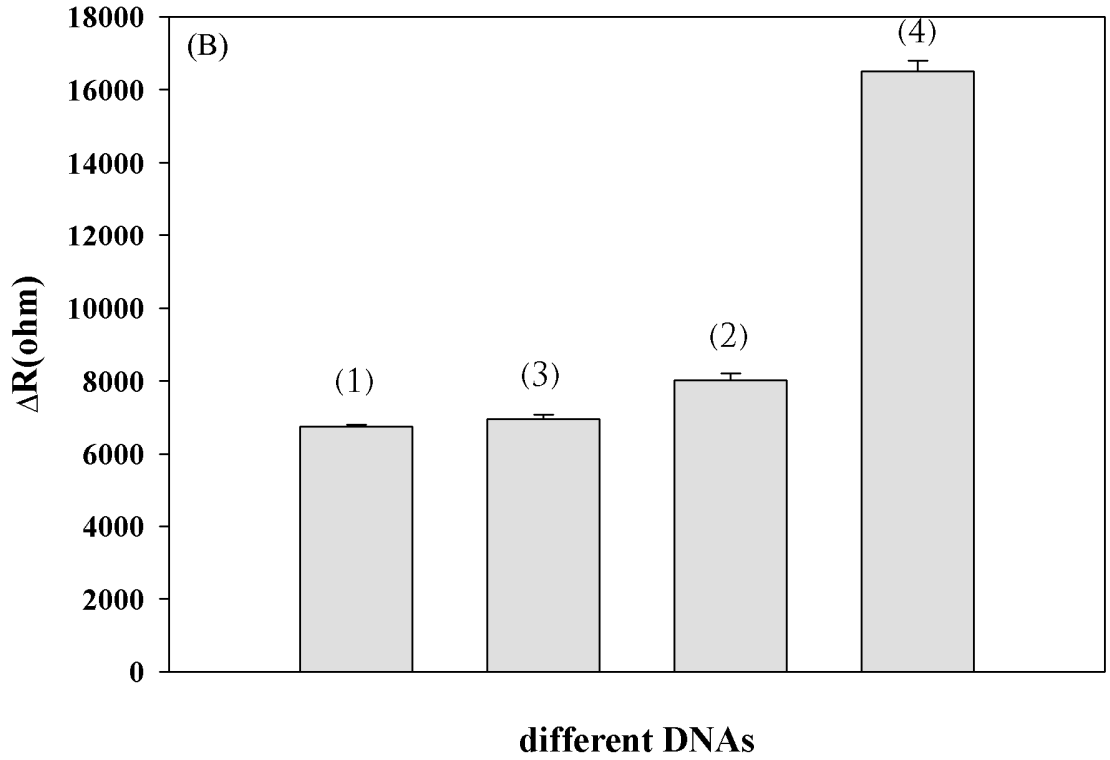

834
835
836
837
838
839

840 Fig. 12
841

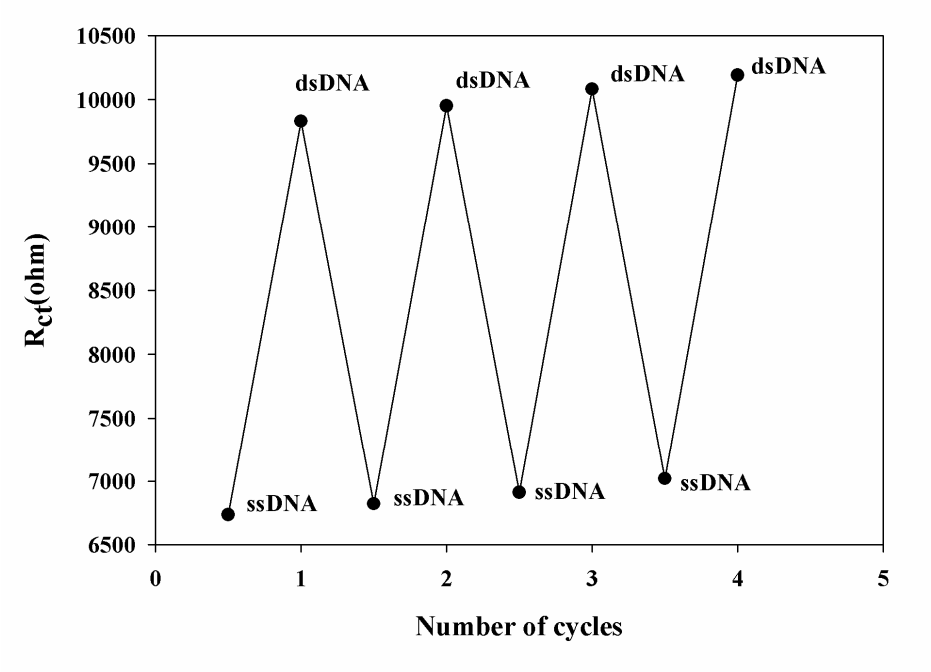

842
843
844
845 Table 1. Comparison between the proposed and other reported biosensors for the detection of
846 *TP53* gene mutation.
847

Electrode materials	Technique	Detection limit (nmol. L^{-1})	Linear range (µmol. L^{-1})	Ref.
Gold electrode	DPV[a]	0.1	-	[10]
CPE[b]	Chronoamperometry	80	0.04-0.15	[9]
SPE[c]	DPV	0.03	5.0×10^{-5}-2.0×10^{-4}	[41]
Gold electrode	DPV	0.68	0.001-0.01	[42]
A-MWCNT/AuNps/Ta	EIS[d]	1.0×10^{-8}	1.0×10^{-9}-0.1	This work

[a] differential pulse voltammetry, [b] carbon paste electrode, [c] screen printed electrode, [d] Electrochemical impedance spectroscopy

848